Bose–Einstein condensation in a QUIC trap

Baolong Lu and William Arie van Wijngaarden

Abstract: The apparatus and procedure required to generate a pure Bose–Einstein condensate (BEC) consisting of about half a million ^{87}Rb atoms at a temperature of <60 nK with a phase density of >54 is described. The atoms are first laser cooled in a vapour cell magneto-optical trap (MOT) and subsequently transferred to an ultra-low pressure MOT. The atoms are loaded into a QUIC trap consisting of a pair of quadrupole coils and a Ioffe coil that generates a small finite magnetic field at the trap energy minimum to suppress Majorana transitions. Evaporation induced by an RF field lowers the temperature permitting the transition to BEC to be observed by monitoring the free expansion of the atoms after the trapping fields have been switched off.

PACS Nos.: 03.75.Fi, 05.30.Jp, 32.80.Pj, 64.60.–i

Résumé : Nous décrivons ici l'appareil et la méthode pour générer un pur condensat de Bose–Einstein (BEC) contenant à peu près un demi million d'atomes de ^{87}Rb à une température <60 nK et une densité de phase >54. Les atomes sont d'abord refroidis par laser dans une vapeur contenue dans un piège magnéto-optique (MOT) et ensuite transférés dans un MOT à pression ultra basse. Les atomes sont chargés dans un piège QUIC, consistant en une paire de bobines quadripolaires et une bobine Ioffe qui génère un petit champ magnétique fini à l'énergie minimale du piège, afin de supprimer les transitions de Majorama. L'évaporation induite par un champ RF abaisse la température, permettant la transition vers le BEC, observée en mesurant l'expansion libre des atomes après que les champs pièges sont éteints.

[Traduit par la Rédaction]

1. Introduction

Bose–Einstein condensation (BEC) is a macroscopic manifestation of quantum mechanics that was first proposed nearly 80 years ago [1–4]. It occurs when the distance between atoms is comparable to their de Broglie wavelength. The exact criteria for a BEC to occur for a three-dimensional gas in free space is

$$n \left(\lambda_{dB} \right)^3 > 2.612 \tag{1}$$

where n is the atom density and λ_{dB} is the de Broglie wavelength, which is given by

$$\lambda_{dB} = \frac{h}{(2\pi M k_B T)^{1/2}} \tag{2}$$

B. Lu and W.A. van Wijngaarden.[1] Physics Department, Petrie Bldg., York University, 4700 Keele St. Toronto, ON M3J 1P3, Canada.

[1]Corresponding author (e-mail: wavw@yorku.ca).

Here, h is Planck's constant, M is the atom mass, k_B is Boltzmann's constant, and T is the temperature. For a dilute atomic gas of rubidium atoms having a density of $\approx 10^{13}$ atoms/cm^3, the temperature to satisfy criterion (1) must be less than 100 nK, which is orders of magnitude lower than that achievable using cryogenic techniques. For atoms contained in a trap having a harmonic potential given by

$$V = \frac{M \left(\omega_1^2 x^2 + \omega_2^2 y^2 + \omega_3^2 z^2 \right)}{2} \tag{3}$$

the BEC transition temperature T_c is given by

$$k_B T_c = 0.15 h \varpi N^{1/3} \tag{4}$$

where $\varpi = (\omega_1 \omega_2 \omega_3)^{1/3}$ and N is the number of atoms [4].

The development of laser-cooling techniques [5] including the development of the so-called magneto-optical trap [6] led to the discovery of new cooling mechanisms such as polarization gradient cooling [7]. This permitted the achievement of relatively dense samples of cold atoms. Alkali atoms were suitable for study as they have transitions where lasers readily operate. [87]Rb in particular was desirable as relatively inexpensive diode lasers generate powers of several hundred milliwatts at the D2 line wavelength of 780 nm.

Magnetic quadrupole traps, created using a pair of coils operated in the so called anti-Helmholtz configuration, have been very useful for trapping and compressing atoms having a magnetic moment. A limitation, however, is that the spin can flip, undergoing a so-called Majorana transition in the region where the field is zero, to an untrapped magnetic hyperfine state inducing a loss and a possible heating mechanism. This difficulty was overcome using several different trap configurations that permitted the attainment of BEC [8–10]. BEC was first observed using the so-called TOP trap [8] that applies a rotating magnetic field. Its drawback is that the trapping fields are not static. An alternative was the cloverleaf magnetic trap that was used to observe BEC in Na [9]. A disadvantage of this technique is that the magnetic fields require currents of several hundred amps that can be switched off in millisecond time intervals [11]. An added difficulty is that these coils have a complicated design and must be cooled in vacuum. A trap having a simpler magnetic coil configuration was the so called QUIC trap developed by the Hänsch group [12, 13]. It consists of a quadrupole trap made with a pair of anti-Helmholtz coils and a third coil known as the Ioffe coil. The latter generates a small magnetic field at the trap minimum. The advantage of the QUIC trap is that much lower currents are required and the coils can remain outside the vacuum. Convenient optical access is also available for laser beams.

The preceding traps have enabled Bose–Einstein condensates to be used to observe atom interference [14] and produce coherent beams of atoms or so-called atom lasers [15]. They have also been used to manipulate the speed of light [16]. Recently, pure optical traps have been developed to obtain BEC in cesium and ytterbium [17, 18]. These traps require relatively high-power laser beams.

The technology to generate a BEC requires extensive control of the frequency, power, and polarization of the laser beams as well as the timing of multiple laser pulses. An ultra-low vacuum of less than 1×10^{-10} Torr (1 Torr = 133.322 Pa) is essential, as collisions with the background gas must be minimized to avoid heating. Finally, the exact timing for integrating the myriad of laser pulses, magnetic fields, and RF evaporation is critical. Every group has developed its own characteristic recipe for generating BEC that is not always apparent. This paper provides the necessary details to show exactly how [87]Rb can be Bose–Einstein condensed in a QUIC trap.

2. Apparatus

2.1. Vacuum system

The creation of a dense sample of ultracold atoms necessary to attain BEC was done using a vacuum chamber consisting of two parts as illustrated in Fig. 1. The upper part was a rubidium vapour

Fig. 1. Vacuum chamber layout.
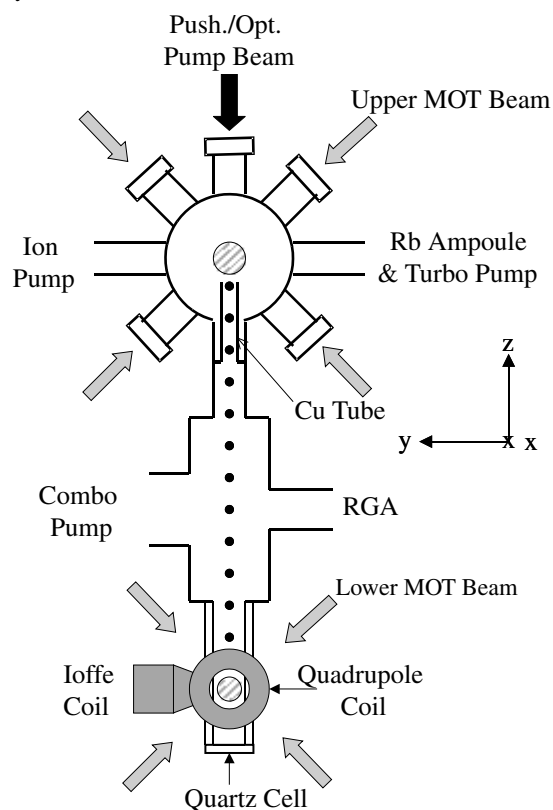
cell maintained at a pressure of about 1×10^{-7} Torr by heating a 5 gm rubidium ampoule (Strem Chemicals). The atoms were first laser cooled in a so-called magneto-optical trap (MOT) and later directed into a second MOT located in the lower chamber by a "pushing laser" pulse propagating downwards in the $-z$ direction. The distance between the upper and lower MOTs was 76 cm. This second chamber was maintained at a pressure of about 2×10^{-11} Torr.

The upper vacuum chamber was custom designed having 10 ports mating to $2.75''$ (1 in = 2.54 cm) diameter conflat flanges. It was connected to a turbo molecular pump (Varian V250) and an ion pump (Varian 929-5000) that had speeds of 250 and 20 L/s, respectively. A turbo molecular pump was used rather than a diffusion pump to avoid oil contamination. The upper chamber was connected to the lower chamber using a 15 cm long, 8 mm diameter copper tube that facilitated differential pumping of the two chambers. The lower chamber consisted of a four-way cross mounted to 15.2 cm diameter conflat flanges. One port was connected to a residual gas analyzer (Stanford Research Systems) that monitored the composition of gases having masses in the range 1 to 200 amu. A second port was connected to a so-called combination pump (Varian Vacion plus 150 Starcell) that consisted of an ion pump having a speed of 150 L/s and a titanium sublimation pump that was surrounded by a cylindrical liquid nitrogen trap.

The bottom of the four-way cross was connected to a conflat flange onto which was fused a rectangular quartz cell (Hellma Cells) having dimensions of $3 \times 3 \times 12.5$ cm^3 with the long dimension oriented in the z direction. The quartz windows had a thickness of 3 mm. The sides of the quartz cell as well as all optical windows and all optical components such as lenses were antireflection coated to minimize laser scatter to less than 0.5% at 780 nm. A straight connector vacuum tube distanced the combination pump 0.5 m away from the quartz cell. This prevented the ion-pump magnets from interfering with the

Fig. 2. Relevant [87]Rb energy levels and laser transitions.
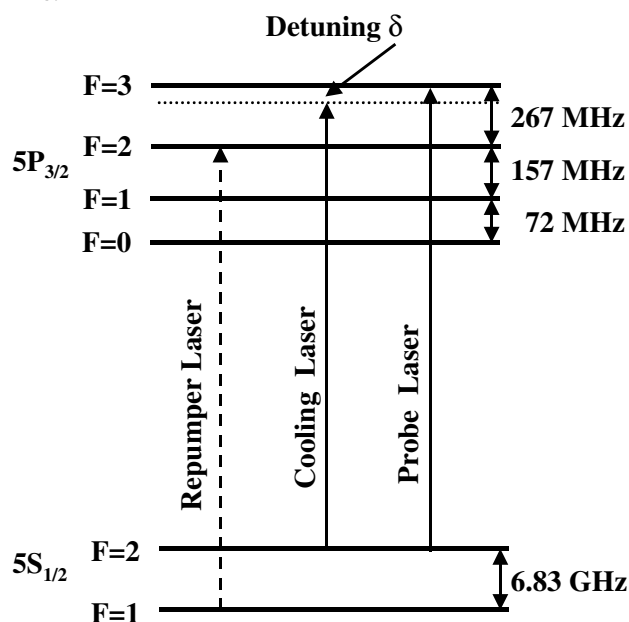
fields generated by the QUIC trap coils that surrounded the quartz cell.

The vacuum system pumping down procedure was as follows. First, the turbo molecular pump reduced the pressure to 1×10^{-7} Torr. The upper and lower ion pumps were then turned on and a mechanical gate valve was closed isolating the turbo pump. The entire vacuum system was wrapped in aluminum foil and baked at a temperature of 100 ° C. The heaters were turned off after 1 week and the vacuum was examined using the residual gas analyzer. Heating was resumed for several additional days if water vapour was detected. The residual pressure of 4×10^{-10} Torr was nearly entirely due to hydrogen that is believed to outgas from the stainless steel vacuum walls. The ion pumps were left on continuously over the several months during which the experiments were done.

The titanium sublimation pump was turned on immediately before atoms were to be trapped in the lower vacuum chamber. The pressure as measured by the ion-pump current, immediately dropped off the scale whenever titanium was sublimated onto the walls of the liquid nitrogen trap. Titanium was sublimated every 30 min during the actual running of the experiment and the liquid nitrogen trap was refilled every 1 h.

2.2. Laser systems

Three different laser systems, called the cooling, repumping, and probe lasers were used in our experiment. Figure 2 illustrates the transitions used to laser cool and trap rubidium atoms. The so-called cooling laser was detuned an amount δ below the [87]Rb $5S_{1/2}$ $(F = 2) \rightarrow 5P_{3/2}$ $(F = 3)$ transition frequency where F denotes the hyperfine level. The repumper laser prevented accumulation of atoms in the $5S_{1/2}$ $(F = 1)$ ground-state hyperfine level by exciting this level to the $5P_{3/2}$ $(F = 2)$ level. The probe laser was resonant with the $5S_{1/2}$ $(F = 2) \rightarrow 5P_{3/2}$ $(F = 3)$ transition.

The three lasers were all mounted on the same optical table whose layout is illustrated in Fig. 3. The repumper and cooling lasers were enclosed in a laminar air flow region (Laminaire Model LP24) to avoid dust accumulation on optical surfaces and thereby reduce maintenance. The cooling laser beam was generated using a diode laser (TuiOptics TA 780) that consisted of a laser oscillator and amplifier that

Fig. 3. Layout of laser systems on optical table.
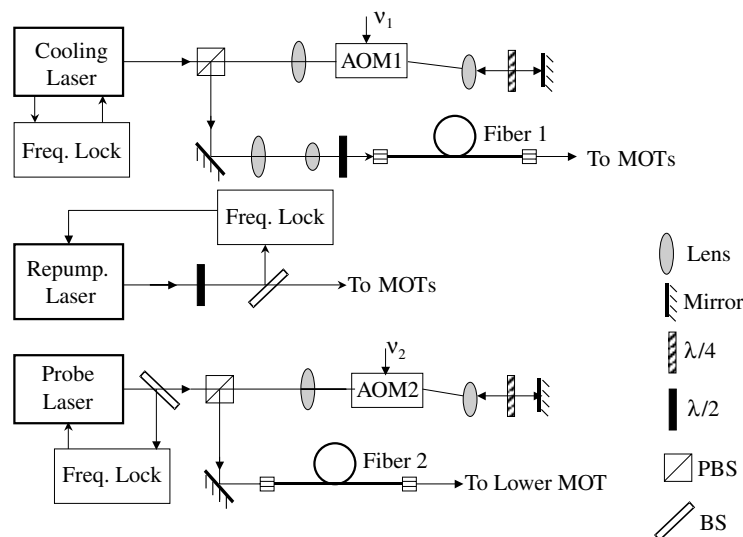
Fig. 4. Apparatus for frequency-locking laser using saturation absorption.
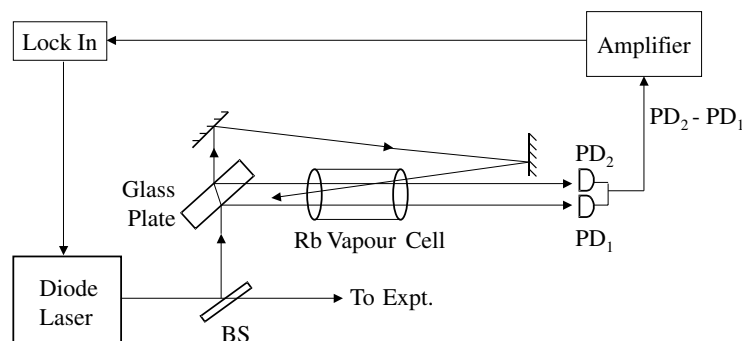
produced 400 mW of light at 780 nm and had a linewidth of 1 MHz. Two optical isolators each having 60 dB suppression were located after the oscillator and amplifier to prevent amplification of backscattered laser light that could otherwise damage the laser components. The laser beam was linearly polarized in the horizontal direction and had a diameter of about 5 mm.

The three lasers were each separately frequency-locked using a saturated absorption signal obtained using a rubidium vapour cell as is illustrated in Fig. 4. Part of the TA780 laser beam generated in the oscillator was directed onto a 12.5 mm thick glass plate. The two surfaces each reflected part of the laser beam through a vapour cell maintained at room temperature. The vapour cells were made of Pyrex™ and were cylindrical in shape having a length of 5 cm and a diameter of 2.5 cm. The cells were attached to a vacuum system that was baked overnight at several hundred degrees Celsius to remove impurities before rubidium was distilled into them. A torch then melted the glass allowing the cells to be removed from the vacuum system.

The saturated absorption signal was obtained using two photodiodes PD_1 and PD_2 (Hamamatsu S5821-03) to monitor the transmission of the two laser beams through the cell. One laser beam intersected a counter-propagating laser beam in the rubidium cell. Hence, PD_1 and PD_2 detected the Doppler-broadened and saturated-absorption spectra, respectively. The difference between the two sig-

Fig. 5. Saturation absorption spectrum. The various peaks are due to transitions between the hyperfine levels F of the ^{87}Rb $5S_{1/2}$ and $5P_{3/2}$ states.
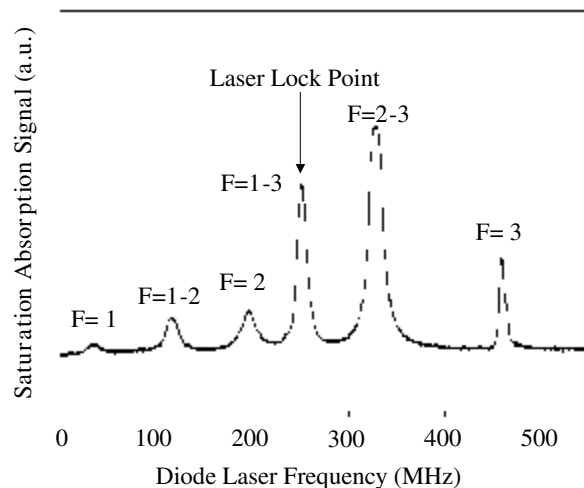
nals removed the Doppler-broadened background yielding a spectrum where the peak widths were comparable to the 5.8 MHz natural line width as shown in Fig. 5. This signal was then amplified and input into a lock-in amplifier. The reference frequency to the lock-in was a 10 kHz signal that modulated the diode laser frequency. The lock-in generated a correction signal to lock the laser to the desired saturated absorption peak using the Hall Pound Drever technique [19]. The TA780 and probe lasers were each frequency locked to the $F = 1 - 3$ cross-over peak shown in Fig. 5 with a frequency stability of better than 1 MHz.

The cooling laser beam was focused back and forth through an acousto-optic modulator using two 50 cm focal length lenses and a mirror as shown in Fig. 3. The acousto-optic modulator (AOM1 IntraAction ATM-100A2) shifted 80% of the laser light by 83.5 to 98.5 MHz on each pass. The AOM1 modulation frequency was generated by the AO driver and monitored by a frequency counter (Optoelectronics 2810). This produced a laser beam detuned 15 to 30 MHz below the $5S_{1/2}$ ($F = 2$) $\rightarrow$ $5P_{3/2}$ ($F = 3$) transition frequency as shown in Fig. 2. The laser polarization direction was rotated into the vertical direction as the laser passed twice through a quarter wave plate (λ/4 Meadowlark RQM-100-780). A 2.5 cm polarizing cubic beamsplitter (PBS – Melles Griot) then reflected the frequency-shifted light. The laser beam was next collimated using a telescope, consisting of 15 cm and 10 cm focal length lenses, into a fiber. A half-wave plate (λ/2 Meadowlark RHM-100-780) rotated the input laser beam polarization axis to optimize fiber transmission.

The repumping laser consisted of a TuiOptics DL 100 followed by a 40 dB optical isolator (Optics for Research IO-5-780-LP) that is not shown in Fig. 3. It generated 30 mW of linear polarized light. Part of the laser beam was reflected by a glass slide and used to frequency lock the laser to the ^{87}Rb $5S_{1/2}$ ($F = 1$) $\rightarrow$ $5P_{3/2}$ ($F = 2$) transition using the saturation spectroscopy technique previously described.

The probe laser (New Focus Model 6018) had a power of 10 mW and was linearly polarized. The laser beam was passed back and forth through an acousto-optic modulator AOM2 identical to AOM1 as illustrated in Fig. 3. This device frequency shifted the laser by 106 MHz on each pass. The laser was then reflected by a PBS and input into a 6 m fiber OFR FCPP-632-6M-FC/APC/APC that transmitted 1.6 mW of the laser power. Probe laser pulses of varying power were generated by adjusting the amplitude of the modulation signal sent to AOM2.

Fibers transported the cooling and probe laser beams from the optical table to the optics surrounding the vacuum system. This ensured that any change in alignment of the optical elements on the laser table did not necessitate readjusting the multitude of subsequent optical components. Mirrors instead of a

Fig. 6. Generation of laser beams for trapping atoms. The broken-line box enclosed optics located on the lower optical breadboard used to generate the lower MOT. Various symbols are the same as defined in Fig. 3.
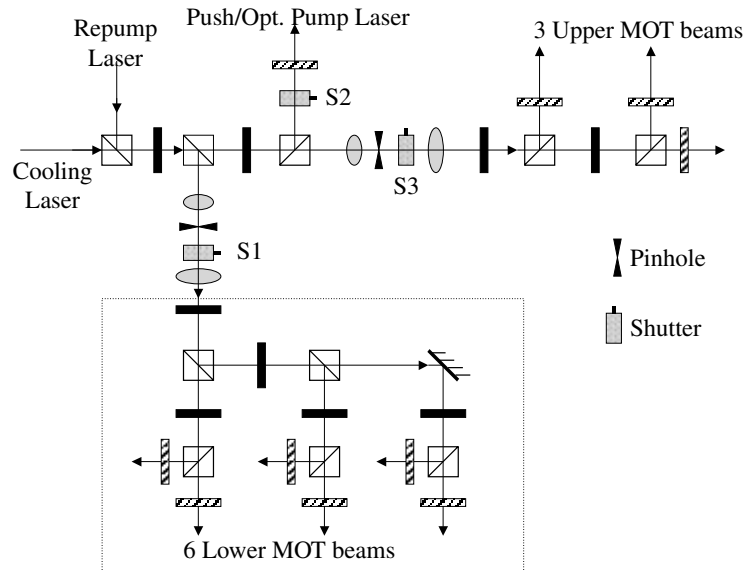

fiber directed the repumper laser as its alignment was not as critical. In the case of the cooling laser, the fiber was a 6 m long single mode polarization maintaining fiber (OFR FCpp-780-6M-FC/PC/PC). The fiber end was adjusted using positioners in the horizontal and vertical directions as well as two angular tilt controllers. Only about 40% of the laser light could be coupled into the fiber, as the input laser beam did not have a Gaussian intensity distribution. The laser beam exiting the fiber had a power of 86 mW.

Figure 6 shows the optical mounts surrounding the vacuum system. All optical mounts were securely fastened to an upper and lower breadboard to minimize vibrations. The cooling laser beam emerging from the fiber was divided into two beams. Initially, this was done using a half-wave plate located before the PBS. It was then noted that the power of either the laser beam transmitted or reflected from the PBS varied by up to ±20% over several hours as is shown in Fig. 7a. This made it difficult to generate six equal-power laser beams for the lower MOT. The problem was that the fiber converted a few percent of the incident linearly polarized light into the orthogonal polarization. This can be caused by temperature-dependent stresses in single-mode fibers [20]. The two orthogonally polarized components emerging from the fiber are apparently coherent. Hence, when the half-wave plate rotated the laser polarization axis and the PBS split the incident laser beam, substantial variations in laser power of the reflected or transmitted laser beam were evident. The solution was to first pass the light emerging from the fiber through a PBS to discard the stray laser polarization component induced by the fiber. The fiber output end was then aligned to optimize the transmission of the dominant polarization component and the laser power monitored after the beamsplitter was very stable as is shown in Fig. 7b.

The MOT laser beams were generated by first combining the repumper and cooling laser beams using a PBS as shown in Fig. 6. A half-wave plate and PBS next divided the laser power such that 36 mW was used to generate the upper MOT laser beams and the pushing laser beam while the remaining 50 mW was used to generated the lower MOT beams. The pushing/optical pumping beam was generated using a half-wave plate and a shutter (Uniblitz LS6T2), which has a diameter of 6 mm and an open/closing time of less than 1 ms. The cooling laser beams for the upper and lower MOT passed through a spatial filter consisting of 5 cm and 35 cm focal length lenses and a 50 μm diameter pinhole. This produced a laser beam having a uniform intensity over a circular area having a 1.5 cm diameter.

Fig. 7. Power stabilization of the laser beam emerging from the fiber. (*a*) Shows the laser power measured after the laser beam, exiting the fiber, first passed through a half-wave plate and was split by a polarizing cubic beamsplitter (PBS). In (*b*) the laser beam exiting the fiber was first incident on a PBS that discarded the small anomalous polarization component generated in the fiber. This stabilizes the power as is discussed in the text.
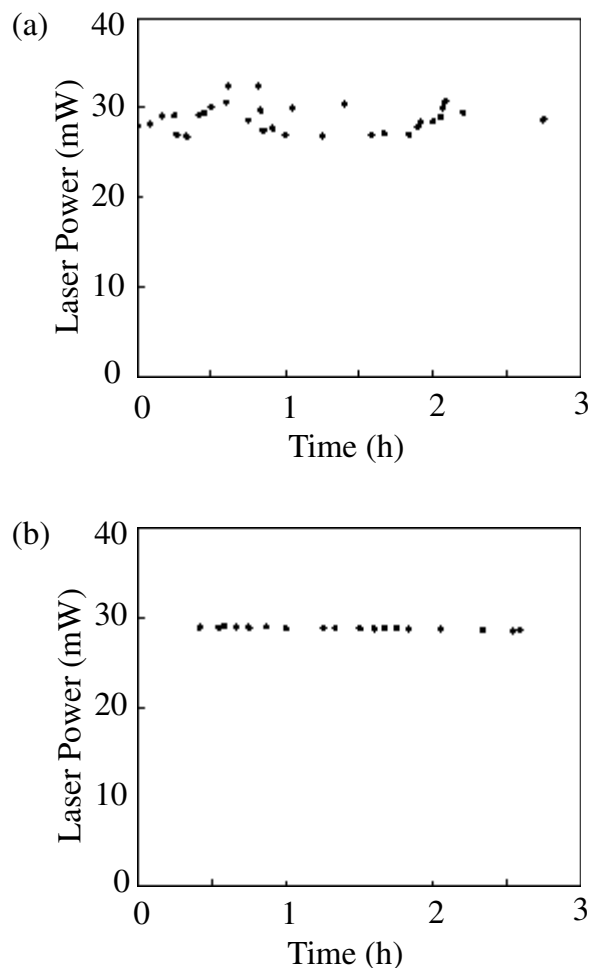
2.3. Computer control

A computer (IBM Pentium III) controlled the experiment using the Labview software program (National Instruments 6.1). The computer was interfaced to the apparatus using a National Instruments interface (PCI-6733) consisting of 8 analog channels and 8 digital channels that controlled the various devices as listed in Table 1.

3. Procedure

The procedure to generate a BEC is given in Table 2. The various steps will now be described.

3.1. Upper MOT

The upper MOT was generated using three circularly polarized laser beams, each having a power of 12 mW, that are illustrated in Fig. 6. The laser beams were retro-reflected to form three pairs of counter-propagating laser beams. The directions of four of these laser beams are shown in Fig. 1, while

Table 1. Computer interface connections.

Analog channel	Function	Digital channel	Function
1	Optical pumping bias field	1	Upper MOT current
2	Lower MOT coil current	2	Shutter S1
3	Ioffe coil current	3	Shutter S2
4	AOM1 frequency	4	Shutter S3
5	AOM1 amplitude	5	RF evaporation trigger
6	AOM2 amplitude	6	2 flipper mirrors
		7	CCD trigger

Table 2. Procedure for generating a Bose–Einstein condensate.

| Time interval	Action
60 s	Trap atoms in upper MOT and push atoms into lower MOT
20 ms	Compress lower MOT cloud
4 ms	Cool atoms using polarization gradient cooling
4 ms	Optically pump atoms into trapped sublevel
2 s	Turn on magnetic quadrupole trap current
1.5 s	Turn on Ioffe coil current to create QUIC trap
40 s	Evaporatively cool atoms
18 ms	Free expansion of ultra-cold atoms
0.1 ms	Image ultra-cold atoms measuring probe laser absorption using CCD

the remaining pair travelled along the $\pm x$ axis. The cooling laser frequency detuning δ equalled 15 MHz. The magnetic field was generated using a pair of anti-Helmholtz coils wrapped around the 5 cm diameter vacuum tube. A current of 7 A was used to generate a magnetic field gradient of about 5 G/cm. About 10^8 atoms were laser cooled to a temperature of a few hundred μK and occupied a volume approximately spherical in shape having a radius of 2 mm.

3.2. Transfer of atoms to lower MOT

The lower MOT was generated using six laser beams, each having a power of 8 mW, that were generated as shown in Fig. 6. Special care was taken to equalize the powers of these laser beams to within 3% to generate a symmetric atom cloud in the MOT. The magnetic field was generated by passing a current of 0.75 A through a pair of quadrupole coils, which are described in Sect. 3.1, to produce a field gradient of about 5 G/cm.

Atoms were transferred from the upper to the lower MOT every 200 ms as follows. First, atoms were loaded into the upper MOT for 195 ms. Afterwards, the current to the upper MOT anti-Helmholtz coils was switched off for 5 ms using a circuit that is described in Sect. 3.5. Shutter S3, shown in Fig. 6, was also closed to block the cooling and repumper laser beams going to the upper MOT. Simultaneously, shutter S2 was opened to permit a 5 ms pushing laser pulse to direct the atoms downwards to the lower MOT. The pushing laser pulse power was adjusted to be 0.3 mW by controlling the amplitude of the modulation signal sent to AOM1. The pushing laser pulse had the same frequency as the cooling laser.

The lower MOT fluorescence was imaged using a 5 cm diameter lens located 28 cm from the MOT onto a CCD camera (SpectraSource Instruments). This camera consisted of a 512×512 array of pixels each having a size of $20 \times 20 \mu$m^2. The CCD remained open for 16 ms whenever it was triggered to take a picture. The overall photon detection efficiency was estimated by multiplying the lens solid angle and the CCD manufacturer-specified efficiency at 780 nm (22%) to be about 0.04%. Calibrated neutral density filters were used to check that the CCD signal varied linearly with the fluorescent intensity. The uncertainty in atom number was estimated to be 20% due to the frequency jitter of the laser that caused

Fig. 8. Temporal dependence of number of atoms transferred to lower MOT.
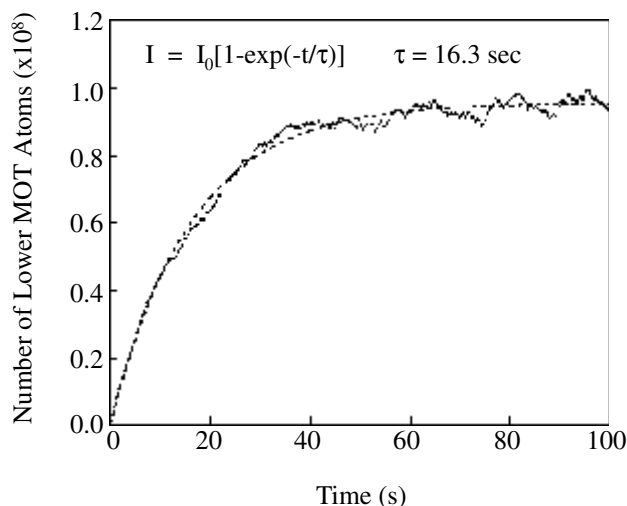
the fluorescence intensity to vary. Figure 8 shows the accumulation of atoms in the lower MOT as a function of time. An exponential function was fit to the data and it showed that the number of atoms increased with a time constant of 16.3 s. Hence, after 60 s, a maximum population of about 10^8 atoms had been loaded into the lower MOT. This represented an overall transfer efficiency between the two MOTs of about 1%.

After 1 min of loading atoms into the lower MOT, the pushing laser beam was shut off. The current in the lower MOT quadrupole coils was increased from 0.75 to 2 A in a 20 ms time interval to compress the size of the atom cloud by a factor of two. A higher field gradient was not used earlier as fewer atoms were then found to be transferred into the lower MOT. The increased magnetic field shifted the Zeeman sublevels increasing the probability an atom can absorb a laser photon. Hence, the cooling laser frequency detuning δ was increased from 15 to 20 MHz to avoid inadvertently heating the atoms.

3.3. Polarization gradient cooling

Polarization gradient cooling is ideally suited to cooling atoms significantly below the so called Doppler limit [7]. It is effective when magnetic fields are absent. Hence, the current to the lower MOT quadrupole coils was switched off. In addition, the Earth's magnetic field was cancelled using three pairs of rectangular coils each having a size of 1 m^2 that surrounded the entire apparatus. A Hall effect gaussmeter measured the residual field at the cell to be less than 20 mG. The cooling laser detuning δ was also increased from 20 to 30 MHz to minimize absorption of the laser beam by the atoms.

Polarization gradient cooling was carried out for a time of 4 ms. The temperature of the atoms was then determined using a 1 ms laser pulse to excite the atoms and the CCD camera to detect the resulting fluorescence. Figure 9 shows the expansion of the atom cloud measured as a function of the time after the end of polarization gradient cooling. A Gaussian function was fit to each image in Fig. 9 to determine the radial position r where the fluorescence is half the peak fluorescence value at the cloud center. r^2 was plotted versus the square of the free expansion time t as shown in Fig. 10. A least-squares fit of a line to the data yielded a temperature of 50 μK.

3.4. Optical pumping

A magnetic trap most strongly traps atoms occupying the ^{87}Rb $5S_{1/2}$ ($F = 2$) $m_F = 2$ sublevel whose magnetic moment is parallel to the magnetic field. Optical pumping enhances the number of trapped atoms by transferring atoms from the other sublevels into the $m_F = 2$ sublevel.

Fig. 9. Free expansion of atom cloud after polarization gradient cooling. Fluorescence was detected using a CCD camera as is described in the text. The atom cloud expanded in time because the atoms have a nonzero temperature and also fell due to gravity.
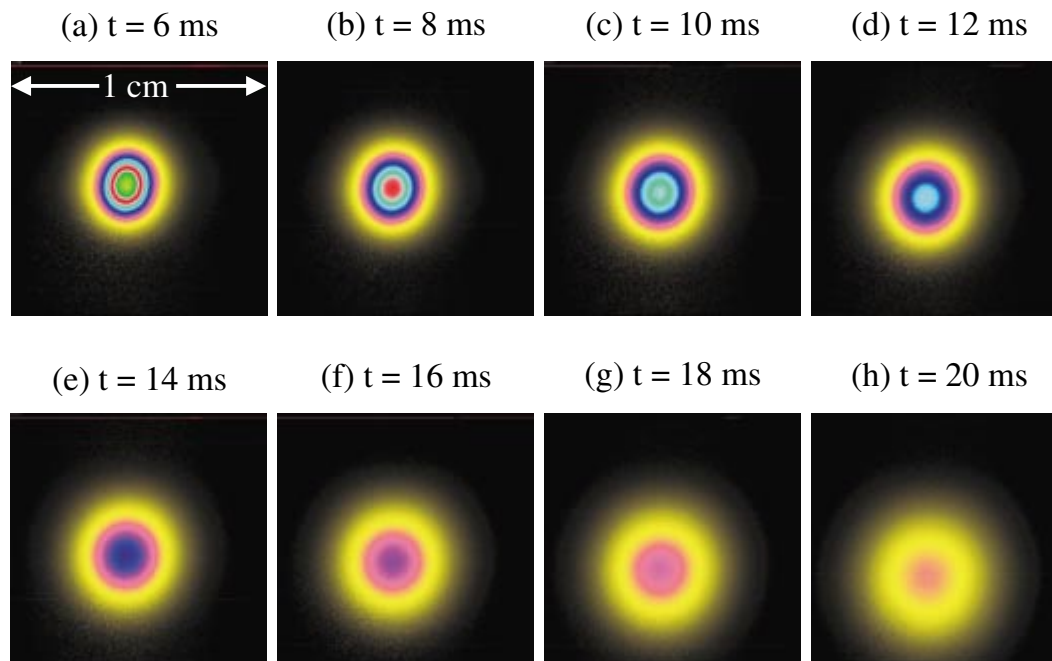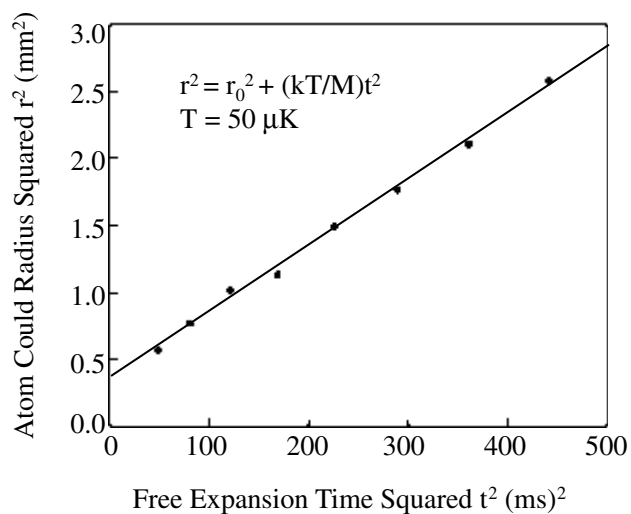
(a) t = 6 ms   (b) t = 8 ms   (c) t = 10 ms   (d) t = 12 ms

(e) t = 14 ms   (f) t = 16 ms   (g) t = 18 ms   (h) t = 20 ms

Fig. 10. Temperature determination of cold atoms.

$$r^2 = r_0^2 + (kT/M)t^2$$
$$T = 50\ \mu K$$

Atom Could Radius Squared r^2 (mm^2)

Free Expansion Time Squared t^2 (ms)^2

Optical pumping was done as follows. First, shutter S1 blocked the cooling and repumper laser beams. A small bias magnetic field of 1.5 G was applied using the pair of coils that otherwise cancel the Earth's magnetic field component in the z direction. Acousto-optic modulator AOM1 and shutter S2 were then used to generate a 30 μW laser pulse having a duration of 1 ms. This time was ample to pump the atoms into the $m_F = 2$ sublevel as the radiative lifetime of the $5P_{3/2}$ state is only 27 ns. The laser beam was circularly polarized and propagated in the $-z$ direction as shown in Fig. 1. Finally, the current

Fig. 11. Lower MOT fluorescence dependence on optical pumping laser power. Fluorescence from the lower MOT was recorded after optical pumping had occurred using a variety of laser powers.
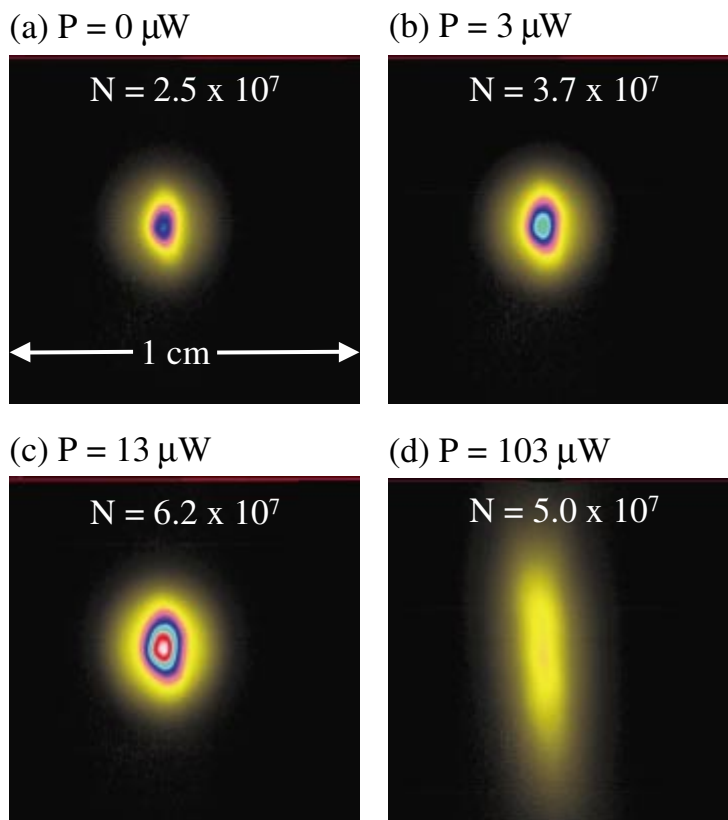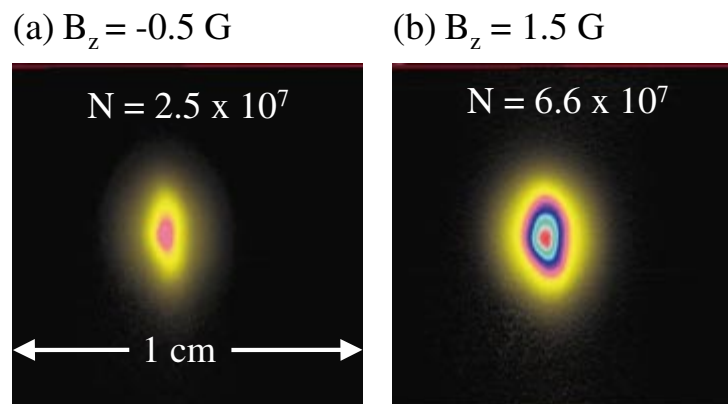
(a) P = 0 μW   (b) P = 3 μW

(c) P = 13 μW   (d) P = 103 μW

Fig. 12. Lower MOT fluorescence dependence on optical pumping bias magnetic field.

(a) B_z = -0.5 G   (b) B_z = 1.5 G

in the quadrupole coil of the QUIC trap was increased from 0 to 12 A to trap the atoms magnetically. Afterwards, the bias field was turned off. It was important to turn on the quadrupole magnetic trap coil current before the bias field was turned off as otherwise there would not be a magnetic field to maintain the orientation of the atomic magnetic moments. A total of 4 ms was required to turn on/off the various

Fig. 13. Configuration of QUIC magnetic trap coils. All dimensions are in millimetres.
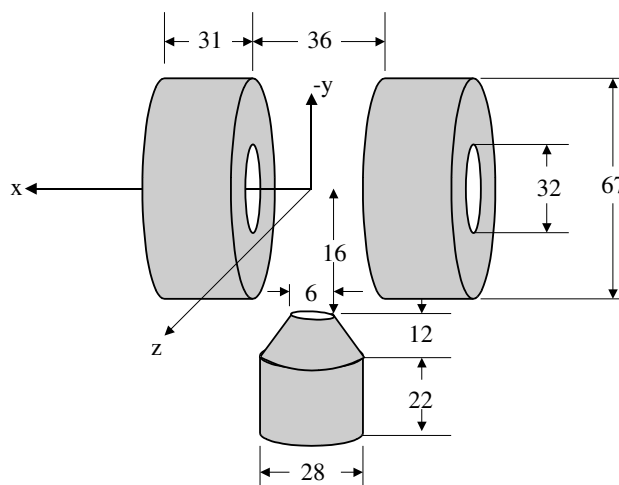
magnetic fields and do the actual optical pumping.

Figure 11 shows the fluorescence produced by atoms in the magnetic trap. The number of trapped atoms more than doubled as the optical pumping laser pulse increased in power. The dependence on the bias field is shown in Fig. 12. Clearly, it is important that the bias field direction be such that atoms are pumped into the magnetically trapped $5S_{1/2} F = 2$ $m_F = 2$ sublevel.

3.5. QUIC trap

Figure 13 shows a schematic drawing of the coils used to generate the QUIC trap. Each quadrupole coil had 181 windings of copper wire having a diameter of 1.7 mm. The Ioffe coil had 238 windings of copper wire having a diameter of 1 mm. The wire windings were fixed into place using thermally conductive epoxy (Omega OB-200-16). Each of the coils was mounted on a water-cooled copper frame. A gap was intentionally left in the frame to prevent eddy currents circulating around the coil frame. These induced currents occur when currents were suddenly switched off and can perturb the trap.

Figure 14 shows the trap depth computed for the coil configuration given in Fig. 13 using a quadrupole coil current of 25 A. The trap minimum shifted from $y = 0$ as the Ioffe coil current I_{IC} increased. The potential well near the minimum in Fig. 14*d* could be approximated by a parabola given by

$$B(y) = B_o + \frac{1}{2} K (y - y_{min})^2 \tag{5}$$

where $B_o = 1.2$ G, $K = 289$ G/cm^2, and $y_{min} = 7.65$ mm.

The currents through the quadrupole coils as well as the Ioffe coil were separately switched on/off in less than 1 ms. Each coil was connected in series to a high-power Mosfet (International Rectifier IRFPS3810) that could withstand up to 580 W of power, and a high-precision sensing resistor. Current conduction across the Mosfet was regulated by a 0 to 10 V signal sent by the computer. The voltage across the sensing resistor enabled a feedback loop to stabilize the current. The sensing resistor consisted of two 0.01 Ω resistors (Precision Resistor PLV10AL0.01) in parallel whose resistance changed by less than 0.1% for currents between 0 and 30 A. A stable sensing resistor was essential as current instability would cause the QUIC trap potential to vary limiting the temperature to which the atoms could be cooled. The current shut-off time was controlled by adding a damping resistor R_D in parallel with each coil that acts as an inductor L. The value of R_D was experimentally determined to ensure the observed current decay time L/R_D was less than 1 ms.

Fig. 14. Modelling of QUIC trap magnetic field. The magnetic fields were computed for the configuration shown in Fig. 13. The current in the quadrupole coil remained constant at 25 A while the Ioffe coil current I_{IC} was varied. Each contour in the diagrams at left represents a field increment of 15 G.
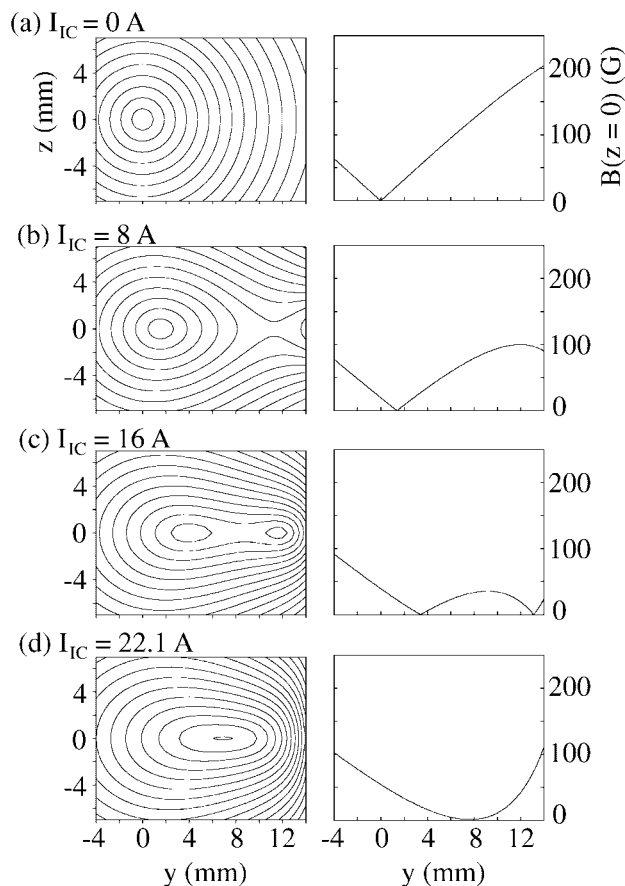

Atoms were loaded into the QUIC trap by first increasing the quadrupole coil current from 12 to 25 A over a 2 s period. This adiabatically compressed the atom cloud facilitating the loading of atoms into the QUIC trap. The Ioffe coil current was subsequently increased from 0 to 22.1 A within 1.5 s. Shutters S1–S3 blocked all laser beams while the currents to the quadrupole and Ioffe coils were increased.

The atoms were studied using a 0.1 ms linearly polarized probe laser beam pulse that travelled through the quartz cell in the $-x$ direction as shown in Fig. 15. The probe laser beam emerging from the fiber was first expanded by a telescope to generate a laser beam having a diameter of 2.5 cm. The probe laser beam next reflected off two 5 cm diameter mirrors mounted on flipper solenoids (New Focus 8892-K) that shifted the mirrors into position in 0.5 s. A 16.5 cm focal length lens then imaged the laser beam onto the CCD camera.

Figure 15b shows a typical picture taken when no cold atoms were present while Fig. 15c shows absorption of the laser beam when 5×10^7 atoms were in the lower MOT. The probe laser power used for these images was less than 1 mW. The probe laser intensity was more than an order of magnitude less than the saturation intensity of the transition. Figure 15d shows an image of the cold atom cloud obtained when Fig. 15b was subtracted from Fig. 15c. The faint background streaks appeared to be due to interference caused by residual laser reflections off the cell walls that were not entirely removed in the background subtraction process.

Figure 16 shows the loading of atoms into the QUIC coil as the Ioffe Coil current was increased.

Fig. 15. Imaging of cold atoms using probe laser absorption. (*a*) illustrates the apparatus while (*b*) shows the signal with no atoms in the QUIC trap, (*c*) shows the signal with 5×10^7 atoms in the trap. (*d*) shows the signal produced after the computer processes the data to subtract the background.
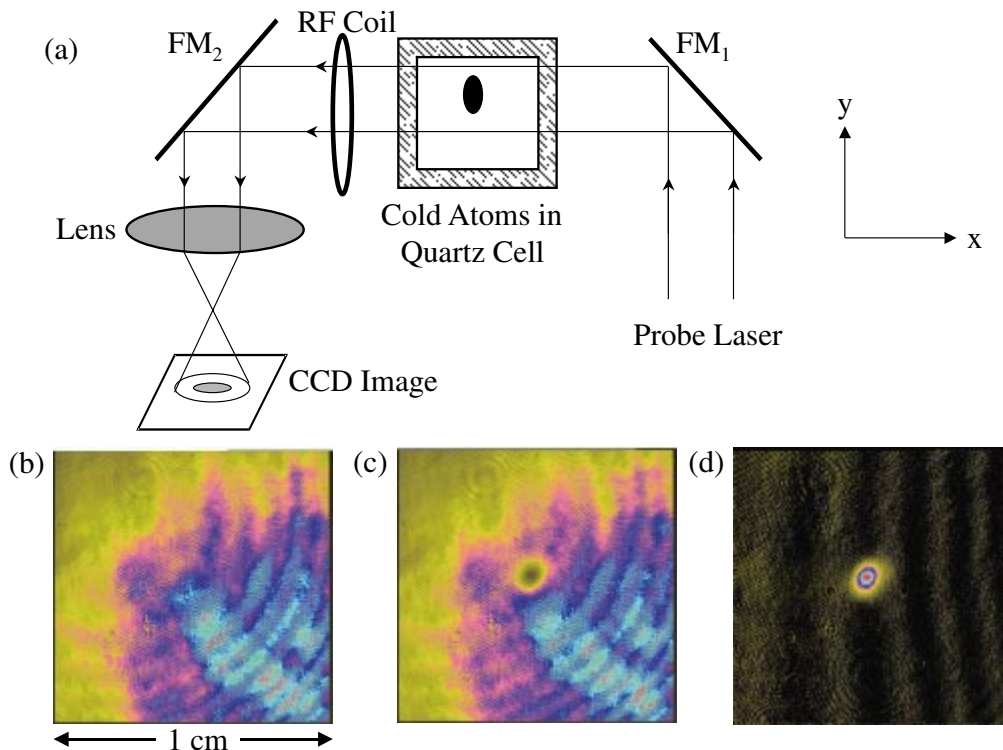

The position of the trapped atoms shifted as expected and there was negligible atom loss. The images in Figs. 16*c* and 16*d* were obtained by shifting the CCD camera 0.5 cm in the *y* direction relative to the position used to take the images shown in Figs. 16*a* and *b*. The atoms remained in the trap for an average of about 100 s as shown in Fig. 17.

3.6. Evaporative cooling

The final stage of cooling was done using an antenna to generate a RF signal whose frequency was swept. The RF radiation flipped the magnetic spins, causing atoms in the trapped $5S_{1/2}$ ($F = 2$) $m_F = 2$ sublevel to undergo a transition to an untrapped sublevel when the RF was resonant with the atoms. The RF frequency, which determines the magnetic field and, therefore, the potential energy at which an atom undergoes a magnetic spin flip and is ejected from the trap, was swept from a high to a low value to force the evaporation of the ensemble at an optimum rate. The shutters S1–S3 blocked all laser beams during this stage of the experiment. Indeed, the entire apparatus was surrounded by black plastic panels to minimize scattered light that could be absorbed by the trapped atoms and cause heating.

The evaporation RF antenna consisted of a single turn of copper wire having a wire diameter of 1 mm and a coil diameter of 2.54 cm. It was positioned 2 cm away from the trap center on the *x* axis as shown in Fig. 15. A 0.2 μf capacitor was added in parallel with the Ioffe coil and also with the quadrupole coils to remove interference due to RF pickup that otherwise affected the magnetic field control circuits. The RF frequency was generated using a synthesized function generator (Stanford Research DS345) and amplified to a maximum power of 10 W by an amplifier (EIN 411LA) having a bandwidth of 300 MHz. The RF frequency ν_{RF} was scanned from $\nu_{start} = 20$ MHz to ν_{stop} in a sweep time T of 40 s. A

Fig. 16. Effect of Ioffe coil current on trapped atom position. The location of the trapped atoms shifted as the Ioffe coil current is increased. The CCD camera and imaging lens were spatially shifted 0.5 cm in the y direction to view the trapped atoms in (c) and (d) as compared to (a) and (b).
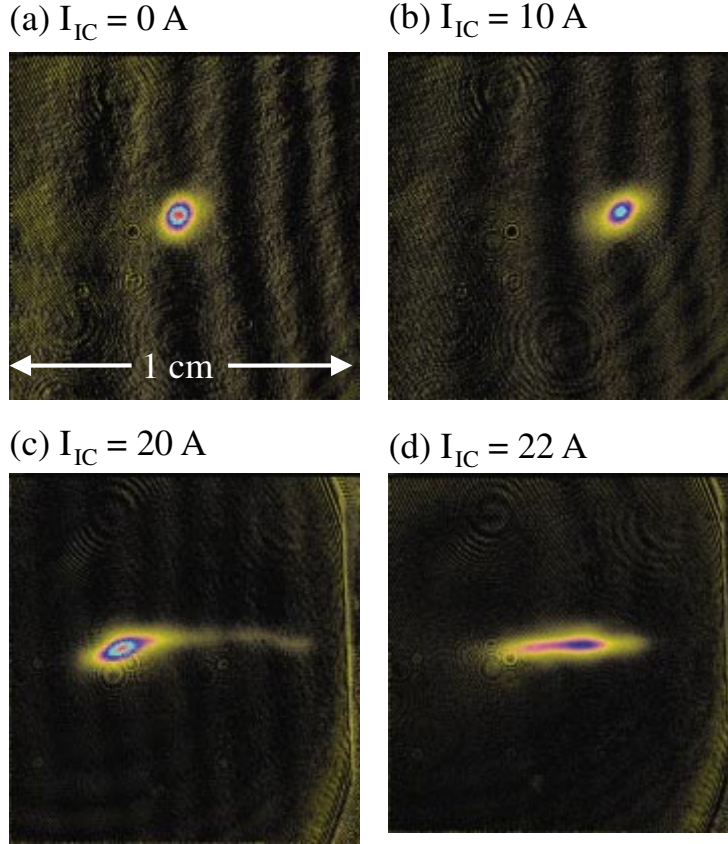
so-called logarithmic scan was used where the frequency ν_{RF} was given by

$$\ln \nu_{RF} = \ln \nu_{start} + \frac{t}{T} \ln \left(\nu_{stop}/\nu_{start}\right) \tag{6}$$

ν_{RF} was scanned more slowly as it approached ν_{stop} since the collision rate decreases as atoms get colder and longer times were, therefore, needed to obtain thermal equilibrium. Finally, the RF was switched on/off by a special computer interfaced switch (Mini Circuits ZYSWA-2-50DR).

The effect of the RF-induced evaporation is shown in Fig. 18 for various stop frequencies using a RF power of 6 W. Here, the atoms were imaged by measuring the absorption of the probe laser beam traversing the cold atom cloud. The RF-induced evaporation reduced the size of the atom cloud with the remaining atoms distributed closer to the energy minimum of the trap. The intensity of the probe laser light propagating in the x direction through the trapped atom cloud is given by

$$I(y, z) = I_o(y, z)\, e^{-\alpha} \tag{7}$$

where I_o and I are the laser intensities before and after interacting with the cold atom cloud, respectively, and α is the optical density. The computer solved (7) giving

$$\alpha(y, z) = -\ln\left[\frac{I(y, z)}{I_o(y, z)}\right] \tag{8}$$

Figure 19 shows that 6 W of RF power was sufficient to maximize the optical depth.

Fig. 17. Temporal dependence of trapped atoms in QUIC trap. This data was taken over a time of 3 h. Some of the scatter of the data points is due to variation in pressure as the titanium sublimation pump was only turned on every half hour.
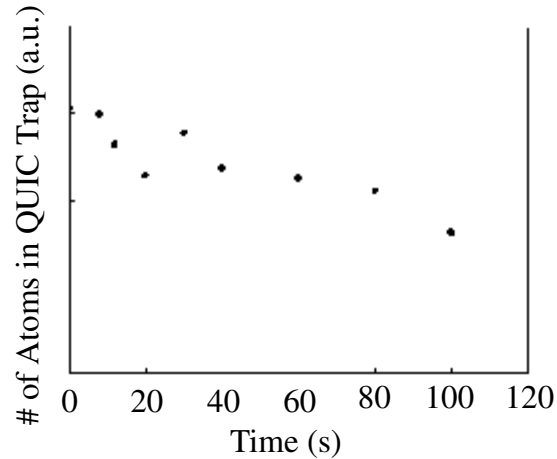

Fig. 18. Evaporation cooling dependence on stop frequency. (*a*) shows the trapped atoms before the 6W RF evaporation signal was applied while the other pictures shows the effect of logarithmically scanning (see text) the frequency beginning at 20 MHz to the stop frequencies indicated.
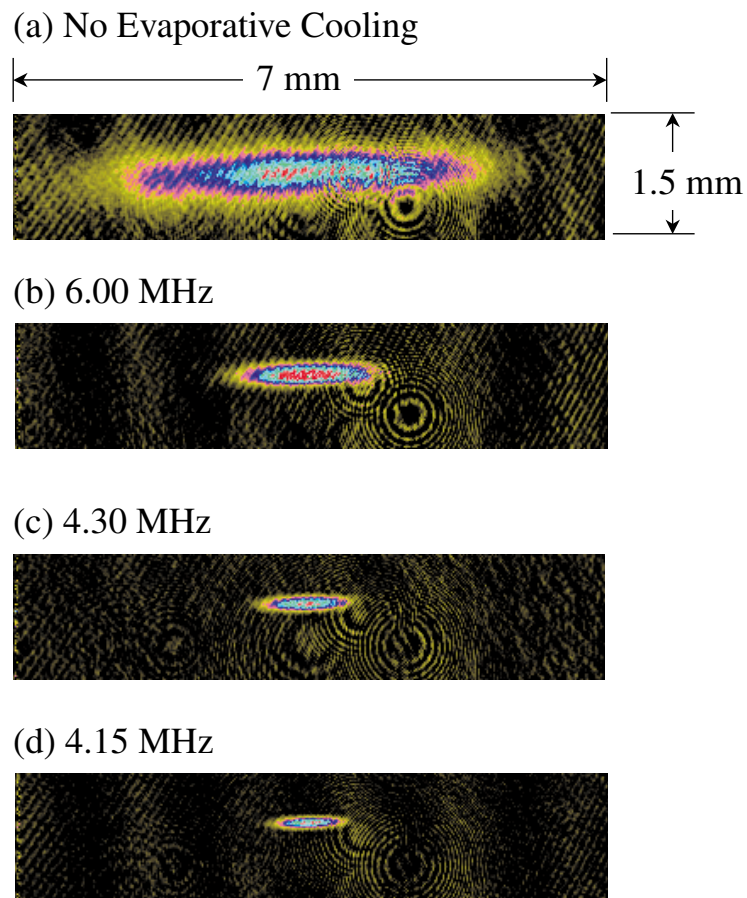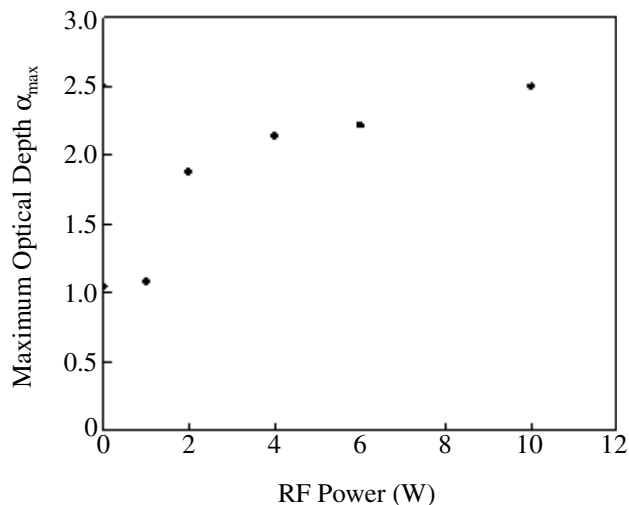
(a) No Evaporative Cooling

(b) 6.00 MHz

(c) 4.30 MHz

(d) 4.15 MHz

Fig. 19. Maximum optical density of cold atom cloud as a function of evaporation RF power. The RF signal was logarithmically scanned from 20 to 4.5 MHz as is described in the text.

3.7. Imaging BEC

The transition to a Bose–Einstein condensate was determined by switching the currents in the QUIC coils off and allowing the atoms to undergo a free expansion for 18 ms following the 40 s evaporation time. The probe laser pulse then traversed the atom cloud and was detected by the CCD camera. A purely thermal cloud is well described by a Maxwellian or Gaussian spatial distribution function that is fitted to the data as is shown in Fig. 20a. Figures 20b and 20c give the corresponding images when the atom cloud has been cooled to lower temperatures using lower values of v_{stop}. The BEC was split into several clouds because the quadrupole and Ioffe coil currents do not damp out with exactly the same time constant [21]. As the magnetic field decreases, the atomic magnetic moments no longer stay aligned and the atoms were distributed among the various sublevels of the $5S_{1/2}$ $F = 2$ hyperfine level. However, the field gradient in the y direction exerted different forces on each sublevel causing the BEC cloud to disperse into several clouds of varying intensity depending on the number of atoms occupying the particular sublevel.

The total number of atoms N was found by integrating the optical depth

$$N = \frac{1}{\sigma} \iint \alpha(y, z)\, dy\, dz \tag{9}$$

and dividing by σ, the cross section for resonant scattering of linearly polarized light, which has been measured for the $5S_{1/2} \rightarrow 5P_{3/2}$ transition to be 1.39×10^{-9} cm^2 [22]. The atom temperature was determined by equating the kinetic energy for motion in the z direction, $(1/2)Mv_z^2$, to $(1/2)k_B T$ where v_z is the velocity component in the z direction. v_z was estimated by measuring the distance for the optical density to decrease to half its value at $z = 0$, which is plotted on the right side of Fig. 20, and dividing by the 18 ms free expansion time. This neglected the initial size of the atom cloud before the free expansion and thus overestimated v_z. Hence, the actual pure BEC temperature was lower than the 100 nK estimate.

An image of the cold atom cloud before the free expansion was made using the laser absorption method described above. The image was distorted due to diffraction effects but did show the atom cloud to have a radius comparable to the CCD pixel width. The size of the cold atom cloud before the free expansion was, therefore, estimated using the trap potential and the atom temperature. The trap-potential

Fig. 20. Transition to BEC. The broken curve is a Gaussian function that was fit to the data. (*a*) Thermal cloud with $N = 3.4 \times 10^6$ atoms at temperature $T = 900$ nK and evaporation stop frequency $\nu_{\text{stop}} = 2.400$ MHz (*b*) Mixed thermal atom cloud and BEC where $N = 1.6 \times 10^6$ atoms, $T = 500$ nK and $\nu_{\text{stop}} = 2.325$ MHz (*c*) Pure condensate where $N = 7.8 \times 10^5$ atoms, $T = 100$ nK, $\nu_{\text{stop}} = 2.315$ MHz. The figures to the right for (*b*) and (*c*) were plotted using the most intense of the clouds in the left pictures. The results were unchanged if any of the other clouds were used.
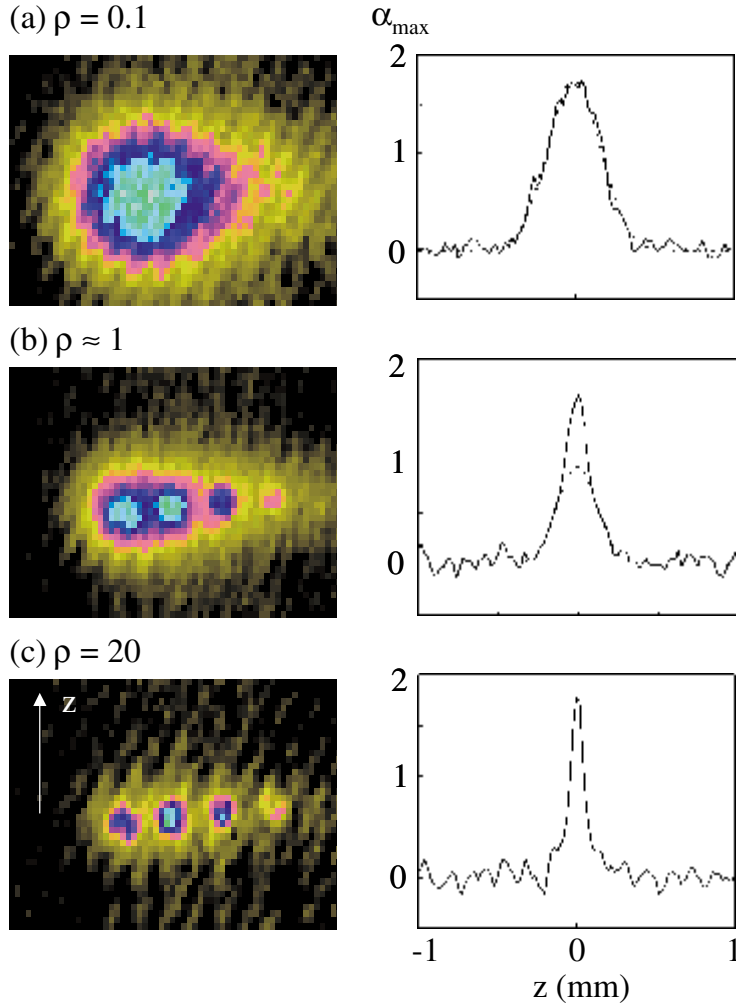

energy U for an atom in the $5S_{1/2}$ $F = 2$ $m_F = 2$ sublevel near the minimum is given using (5)

$$U = \mu_B K r_y^2 \tag{10}$$

where μ_B is the Bohr magneton and $r_y = y - y_{\text{min}}$ is the size of the trapped atom cloud. Equating (10) to $(1/2)k_B T$ gives $r_y = (k_B T / \mu_B K)^{1/2} = 23\mu$m. The size of the cloud in the x and y directions as modeled in Fig. 14 and observed in Fig. 18 was estimated using $r_x \approx r_z \approx r_y/5$. The atom density of an ellipsoidal cloud of atoms was found to be 10^{14} atoms/cm^3 using [23]

$$n = \frac{N}{\left(8\pi^3\right)^{1/2} r_x r_y r_z} \tag{11}$$

Fig. 21. Transition to BEC. This figure is similar to Fig. 20 except that the Ioffe coil current was adjusted to decay more slowly than the quadrupole coil current preventing Majorana spin flips as discussed in the text. (*a*) Thermal cloud with $N = 1.9 \times 10^6$ atoms at temperature $T = 450$ nK (*b*) Mixed thermal atom cloud and BEC where $N = 1.8 \times 10^6$ atoms and $T = 400$ nK (*c*) Pure condensate where $N = 4.2 \times 10^5$ atoms and $T < 60$ nK.
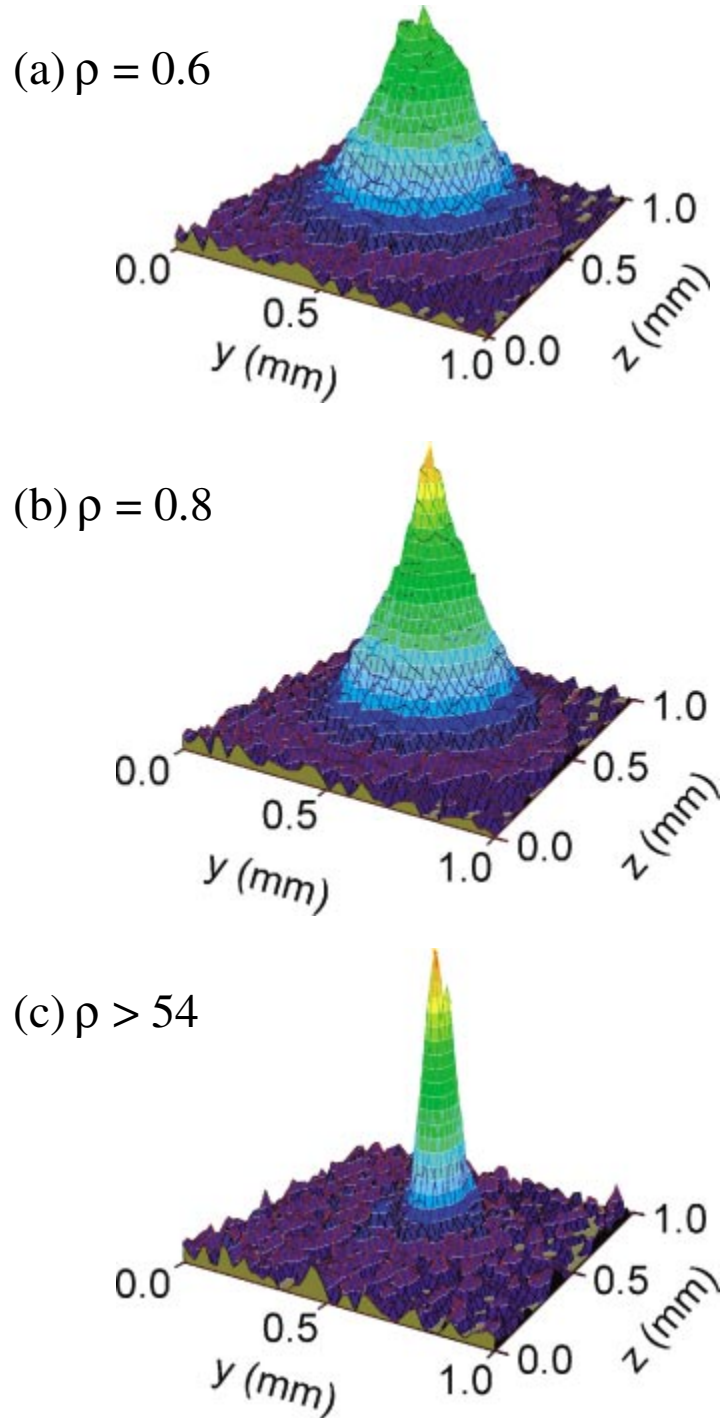
Finally, the phase density is given by

$$\rho = n\lambda_{dB}^3 \tag{12}$$

A phase density of 20 was achieved by scanning the RF to a frequency of $\nu_{stop} = 2.315$ MHz. The number of trapped atoms decreased below this frequency vanishing altogether at 2.304 MHz. This corresponded to a magnetic field at the trap center slightly higher than the calculated value of 1.2 G.

Subsequent to the acceptance of this paper, the electronic circuits controlling the trap currents were adjusted so that the Ioffe-coil current decayed slightly slower than the quadrupole coil current when the magnetic trap was switched off. The atomic spins then did not experience a vanishing magnetic field that caused Majorana transitions and a single peak was observed after the free expansion of the BEC as shown in Fig. 21. These data were taken using a 24 ms free expansion time and progressively lower RF stop frequencies ν_{stop} to cool the atoms.

4. Conclusions

The results of this work are comparable to those obtained in the first demonstration of the QUIC trap [12]. Both experiments used Ioffe and quadrupole coils having similar geometries and currents although Esslinger et al. [12] enclosed the cell in a μ-metal shield. They transferred atoms between the upper and lower MOTs using moving molasses [24, 25]. The latter technique requires precise control of the frequency of two laser beams propagating along the $\pm z$ directions using acousto-optic modulators. In contrast, this experiment used only a single laser beam having the same frequency as the cooling laser to push the atoms out of the upper MOT toward the lower MOT. Esslinger et al. [12] were able to load 10^9 atoms into their lower MOT, which were subsequently loaded into the QUIC trap and evaporatively cooled for 23 s to produce a pure condensate consisting of 5×10^5 atoms. Values of the temperature and phase density of the condensate were not reported. The present experiment loaded 10^8 atoms into the lower MOT, which were evaporatively cooled for 40 s to obtain a pure condensate having 7.8×10^5 atoms at a temperature of 100 nK and a phase density of 20.

The QUIC trap lends itself to relatively convenient studies of BEC since the lower MOT is spatially separated from the location where BEC is formed. This may facilitate the study of tunneling of condensed bosons in an optical lattice as a function of the potential lattice depth [26]. It will also be interesting to explore whether the extremely low temperature of the atoms can be exploited to generate beams of coherent atoms having very low transverse temperatures. Such tightly collimated atomic beams would be of interest for nanolithography [27]. It would be very desirable to significantly increase the number of condensate atoms and decrease the time necessary to create a BEC. Higher power CW lasers such as titanium–sapphire lasers having a high-quality Gaussian spatial mode would enable larger diameter laser beams to trap orders of magnitude more atoms in the initial MOT. The QUIC trap has the advantage over other magnetic traps used to create BEC of requiring smaller coils and lower currents. Hence, it will undoubtedly facilitate future studies and applications of BEC.

Acknowledgements

References

1. S.N. Bose. Z. Phys. **26**, 178 (1924).
2. A. Einstein. Sitzungsberichte der Preussischen Akademie der Wissenschaften, Physikalisch-mathematische Klasse (1924).
3. A. Griffin, D.W. Snoke, and S. Stringari *Editors*. Bose–Einstein condensation. Cambridge University Press, Cambridge. 1995.

4. C.J. Pethick and H. Smith. Bose–Einstein condensation in dilute gases. Cambridge University Press, Cambridge. 2002.
5. H.J. Metcalf and P. van der Straten. Laser cooling and trapping. Springer, New York. 1999.
6. E. Raab, M. Prentiss, A. Cable, S. Chu, and D. Pritchard. Phys. Rev. Lett. **59**, 2631 (1987).
7. J. Dalibard and C. Cohen-Tannoudji. J. Opt. Soc. Am. B, **6**, 2023 (1989).
8. M.H. Anderson, J.R. Ensher, M.R. Matthews, C.E. Wieman, and E.A. Cornell. Science (Washington, D.C.), **269**, 198 (1995).
9. K.B. Davis, M.O. Mewes, M. Andrews, M. van Druten, D. Durfee, D. Kurn, and W. Ketterle. Phys. Rev. Lett. **75**, 3969 (1995).
10. C.C. Bradley, C.A. Sackett, J.J. Tollet, and R.G. Hulet. Phys. Rev. Lett. **75**, 1687 (1995).
11. D. Durfee. Ph.D. thesis. MIT, Cambridge, Mass. 1999.
12. T. Esslinger, I. Bloch, and T.W. Hansch. Phys. Rev. A, **58**, R2664 (1998).
13. J.E. Lye, C.S. Fletcher, U. Kallmann, and J.D. Close. OSA Meeting, Pasadena. 2001.
14. M.R. Andrews, C.G. Townsend, H.J. Miesner, D.S. Durfee, D.M. Kurn, and W. Ketterle. Science (Washington, D.C.), **275**, 637 (1997).
15. M.O. Mewes, M.R. Andrews, D.M. Kurn, D.S. Durfee, C.G. Townsend, and W. Ketterle. Phys. Rev. Lett. **78**, 582 (1997).
16. L. Hau, S.E. Harris, Z. Dutton, and C.H. Behroozi. Nature, **397**, 594 (1999).
17. T. Weber, J. Herbig, M. Mark, H.C. Nagerl, and R Grimm. Science (Washington, D.C.), **299**, 232 (2003).
18. Y. Tahasu, K. Maki, K. Komori, T. Takano, K. Honda, M. Kumakura, T. Yabuzaki, and Y. Takahashi. Phys. Rev. Lett. **91**, 040404 (2003).
19. W. Demtroder. Laser spectroscopy. Springer-Verlag, New York. 1988.
20. D.S. Waddy. IEEE Photon. Tech. Lett. **13**, No. 9, 1035 (2001).
21. J. Stenger, S. Inouye, D.M. Stamper-Kurn, H.J. Miesner, A.P. Chikkatur, and W. Ketterle. Nature (London), **396**, 345 (1998).
22. D.J. Han. Ph.D. thesis. University of Texas, Austin, Texas. 1998.
23. W. Petrich, M.H. Anderson, J.R. Ensher, and E.R. Cornell. J. Opt. Soc. Am. B, **11**, 1332 (1994).
24. M. Kasevich, D.S. Weiss, E. Riis, K. Moler, S. Kasapi, and S. Chu. Phys. Rev. Lett. **66**, 2297 (1991).
25. K. Gibble, S. Chang, and R. Legere. Phys. Rev. Lett. **75**, 2666 (1995).
26. J.J. Liang, J.Q. Liang, and W.M. Liu. Phys. Rev. A, **68**, 043605 (2003).
27. J. McClelland and R.J. Celotta. Thin Solid Films, **367**, 25 (2000).